Available online at www.sciencedirect.com
SCIENCE DIRECT
Journal of Catalysis 241 (2006) 367–377
JOURNAL OF CATALYSIS
www.elsevier.com/locate/jcat

[V,Al]-MCM-22: A novel acid/redox bifunctional molecular sieve

A. Albuquerque [a,b,c], L. Marchese [b], L. Lisi [c], H.O. Pastore [a,*]

[a] *Grupo de Peneiras Moleculares Micro e Mesoporosas, Instituto de Química, UNICAMP, CP 6154, CEP 13084-862, Campinas-SP, Brazil*
[b] *Dipartimento di Scienze e Tecnologie Avanzate, Università del Piemonte Orientale "A. Avogadro", Via Bellini 25G, I-15100 Alessandria, Italy*
[c] *Istituto Ricerche sulla Combustione, CNR, P. le Tecchio, 80 Napoli, Italy*

Received 21 February 2006; revised 3 May 2006; accepted 5 May 2006

Available online 12 June 2006

Abstract

The synthesis and characterization of a novel vanadoaluminosilicate, [V,Al]-MCM-22, with **MWW** structure has been performed. As-synthesized, calcined, and H^+ and Na^+ ion-exchanged materials were characterized by various techniques, including X-ray diffraction (XRD), scanning electronic microscopy (SEM), Fourier transform infrared spectroscopy (FTIR), and thermogravimetric analysis (TGA). The presence of redox sites (V^{4+}/V^{5+} couples) after oxidation in O_2 at 580 °C and reduction in H_2 at 500 °C was monitored by diffuse reflectance (DR) UV–vis spectroscopy and by FTIR of CO adsorption at 100 K. Preliminary catalytic tests on the oxidative dehydrogenation (ODH) of propane provided promising results.

Keywords: [V,Al]-MCM-22; Vanadoaluminosilicates; ODH reaction

1. Introduction

The zeolite MCM-22 (IZA code **MWW**) was first synthesized in the laboratories of Mobil Oil Corporation, using hexamethyleneimine as the structure-templating agent [1]. Its structure is built of two systems of independent channels, both accessible by elliptic windows of 10-membered TO_4 rings (T = Si or Al). The first channel system is composed of sinusoidal 10-membered channels; the second, by the stacking of supercavities, whose internal diameter of 7.1 Å is defined by 12-membered rings with a height of 18.2 Å. Its particular structure, as well as the possibility of delamination [2] or pillarization [3], makes this zeolite very interesting for a series of catalytic reactions.

The isomorphous substitution of heteroatoms in the **MWW** structure has been done sucessfully with Ga [4], Ti [5], and Fe [6]. In all cases, the presence of extra-structural species has been observed, although in small proportions. In the case of Fe-MCM-22, extra-structural Fe^{3+} species may be transformed to Fe^{2+} on a reduction treatment [7]. Ti-MCM-22 has already been used as a catalyst for oxidation of alkenes [8] and epoxidation reactions [9], whereas Ga-MCM-22 has been used in the dehydrogenation of methylcyclohexane [10].

Since the earlier reports on the V-silicalites in the 1990s [11], vanadium ions have been introduced in several zeolite structures, including **MFI**, **BEA**, **MEL**, ZSM-48, and others [11–16]. Multitechnique approaches often have been used to characterize structure, oxidation state, and dispersion of the vanadium species, and, depending on the vanadium loading, various species have been detected. Isolated pseudotetrahedral, square pyramidal, and octahedral V^{5+} and V^{4+} ions, VO^{2+} ions, and V-oxide clusters are the most commonly detected intrazeolite vanadium species [11–16]. The insertion of vanadium ions within zeolite frameworks has been attempted following several preparation routes [11–17]. Besides the hydrothermal direct (one-pot) synthesis, vanadium ions have been introduced in zeolites by exchanging counterions (H^+ or Na^+ ions) with vanadyl ions (VO^{2+}) [12,17,18].

As far as we know, however, no attempt to introduce vanadium ions in the **MWW** framework has been published so far, except for the preliminary data on the characterization of [V,Al]-MCM-22 reported earlier by our group [18,19]. In the

* Corresponding author.
E-mail addresses: leonardo.marchese@mfn.unipmn.it (L. Marchese), lisi@irc.na.cnr.it (L. Lisi), gpmmm@iqm.unicamp.br (H.O. Pastore).

0021-9517/$ – see front matter © 2006 Published by Elsevier Inc.
doi:10.1016/j.jcat.2006.05.012

present work, more extended and detailed synthesis studies, along with tests to characterize the bifunctionality of the molecular sieve, are reported.

2. Experimental

2.1. Synthesis

Synthesis gels of [V,Al]-MCM-22 were prepared in the following composition: 1.0 SiO_2:0.02 Al_2O_3:0.03 $VOSO_4$:0.30 NaOH:0.60 HMI:30 H_2O, where HMI is hexamethyleneimine, the structure-directing agent. The synthesis procedure used was adapted from Marques et al. [20], introducing $VOSO_4$ together with the aluminum source. Hydrothermal treatments were carried out under static conditions at 150 °C for crystallization periods of 48–192 h.

HMI was removed by heating under argon from room temperature to 500 °C at a heating rate of 1 °C/min and maintaining this temperature for 12 h under argon flow. Subsequently, the sample was heated up to 580 °C under argon, and the sample was maintained at this temperature for 6 h under dry oxygen flow. Calcined [V,Al]-MCM-22 was exchanged with Na^+ or NH_4^+ ions (0.1 mol L^{-1} sodium nitrate or ammonium acetate solutions at a ratio of 10 mL of solution/g of zeolite, stirring at 60 °C for 24 h). The exchanged samples were heated up to 500 °C under argon flow, and once the temperature was reached, the gas was changed to dry oxygen and left in these conditions for 6 h. These samples were designated as Na-[V,Al]-MCM-22 and H-[V,Al]-MCM-22.

2.2. Materials characterization

2.2.1. X-Ray diffraction (XRD)

Data were collected for the as-synthesized and calcined samples as hand-pressed wafers on a Shimadzu XRD 6000 diffractometer at room temperature with Cu-K_α radiation, generated at 40 kV and 30 mA from 1.4 to 50° 2θ at a rate of 2° min^{-1} and slits of 0.5°, 0.5° and 0.3 mm for exit, reception and divergence, respectively.

2.2.2. Elemental analysis

Elements concentration was determined by solubilizing the samples by oxidizing alkaline fusion with lithium metaborate. The resulting material was dissolved, and the elements were determined by atomic absorption with a Varian A-5 spectrophotometer, using a nitrous oxide/acetylene flame.

2.2.3. Thermogravimetric analysis (TGA)

Samples were analyzed in a Du Pont 2000 thermal analyser, from 30 to 1000 °C, with a heating rate of 10 °C min^{-1}, under both argon and oxygen flow (100 mL min^{-1}).

2.2.4. Diffuse reflectance (DR) UV–vis spectroscopy

DR UV–vis spectroscopy was carried out on a Perkin Elmer Lambda 900 UV/Vis/NIR spectrophotometer, using a quartz cell that permitted analysis both under vacuum conditions (residual pressure $\leqslant 10^{-5}$ mbar) and under controlled gas atmospheres. Spectra were taken from 190 to 800 cm^{-1}. *Oxidized samples* were obtained by treating the powder directly within the DR–UV–vis cell under O_2 at 580 °C (60–80 Torr for 3 h), and *reduced samples* were obtained under H_2 at 500 °C (60–80 Torr for 3 h); oxidized and reduced samples were finally treated for 30 min under vacuum at 250 and 500 °C, respectively.

2.2.5. Electron paramagnetic resonance (EPR)

EPR spectra of solid samples were recorded at room temperature on a Bruker EMX instrument, operating at a frequency of 9.35 GHz and at a potency of 20.02 mW, with 100 kHz of frequency modulation.

2.2.6. Fourier transform infrared spectroscopy (FTIR)

FTIR analysis was carried out using a Bruker Equinox 55 spectrophotometer equipped with a pyroelectric detector (DTGS type); a resolution of 4 cm^{-1} was adopted. Pelletized as-synthesized [V,Al]-MCM-22 was thermally treated under vacuum by heating from room temperature to 500 °C at 1 °C/min and leaving at this temperature for 12 h. Subsequently, the sample was heated up to 580 °C and dry oxygen was added (60–80 Torr); the sample was maintained at this temperature for 6 h. Oxidized and reduced samples were obtained by the same treatments described above for DR–UV–vis experiments in a quartz cell suitable for adsorption–desorption experiments at room temperature and liquid nitrogen temperature. Temperatures of around 100 K could be attained with this cell [21].

Framework FTIR spectra were registered on a Bomen Michelson MB-102 spectrophotometer, in the 4000–400 cm^{-1} region, with a resolution of 4 cm^{-1} and 16 scannings, using 100-mg KBr pellets with sample concentration of approximately 0.25 wt%.

2.2.7. Scanning electron microscopy (SEM)

SEM was performed on a JEOL 6360LV microscope. The samples were graphite-sputtered on a Bal-Tec MED020 before analysis.

2.3. Catalytic activity measurements

Catalytic activity tests of propane oxidative dehydrogenation (ODH) were carried out in a fixed-bed quartz microreactor operating under atmospheric pressure. The feed composition was 2.5% propane, 5% O_2, and He balance (in volume). The contact time was fixed at 0.11 g h dm^{-3}, and the reaction temperature ranged from 350 to 550 °C. Analysis of hydrocarbons was performed by an on-line Hewlett-Packard HP5890A (series II) gas chromatograph equipped with a Poraplot capillary column and a flame ionization detector (FID). Concentrations of O_2, CO, and CO_2 were measured by an on-line Hartmann & Braun URAS 10 E continuous analyser. Water produced by the reaction was retained by a $CaCl_2$ trap, to avoid condensation in the cold parts of the experimental apparatus.

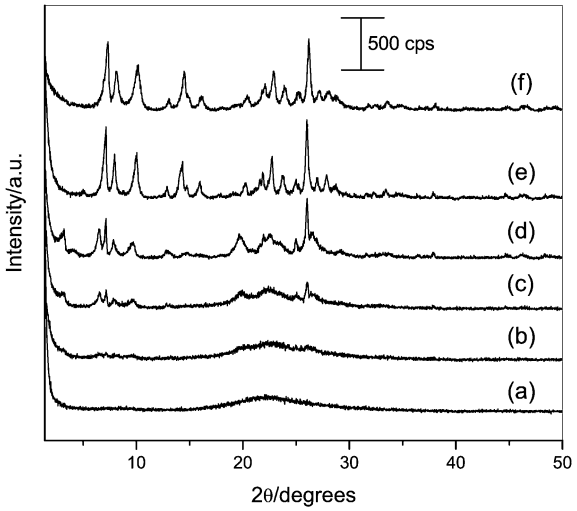

Fig. 1. XRD of as-synthesized [V,Al]-MCM-22 samples crystallized in (a) 48 h, (b) 96 h, (c) 144 h, (d) 192 h and calcined, (e) 192 h [V,Al]-MCM-22 and (f) [Al]-MCM-22 SAR = 34 samples.

3. Results and discussion

[V,Al]-MCM-22 was synthesized using the same procedure as for [Al]-MCM-22 obtained from static synthesis [20] with the addition of vanadyl sulfate together with the aluminum source in one single aqueous solution. Fig. 1 presents XRD data for [V,Al]-MCM-22 obtained in synthesis times varying from 48 to 192 h. The 48-h sample (Fig. 1a) presented only the amorphous phase, whereas after 144 h (Fig. 1c), low-intensity peaks corresponding to the incipient **MWW** structure were observed. Only after 192 h did the sample attain the maximum crystallinity (Fig. 1d). No crystalline-intermediate phases were observed during the crystallization of [V,Al]-MCM-22, meaning that the phase of interest was obtained directly from the gel. Higher crystallization times led to the formation of contaminant phases.

Table 1
Composition of the samples, determined by elemental analysis

	V_2O_5 (wt%)	SiO_2/Al_2O_3	SiO_2/V_2O_5	Al/V	Na/Al
[V,Al]-MCM-22	0.57	40	473	12	0.09
H-[V,Al]-MCM-22	0.25	30	1036	35	0.02
Na-[V,Al]-MCM-22	0.27	34	999	30	0.20
[Al]-MCM-22	–	34	–	–	0.02

Calcined [V,Al]-MCM-22 presented sharper diffraction peaks and a higher degree of crystallinity compared with calcined, vanadium-free [Al]-MCM-22 with SAR = 34: 100% and 91%, respectively (cf. Figs. 1e and f).

As a matter of fact, insertion of V into the [Al]-MCM-22 framework led to a more crystalline material. In general, the incorporation of heteroatoms like vanadium in silicate zeolites decreased the crystallinity of the material [22,23]. However, as the example of [Fe,Al]-MCM-22, introducing a metal atom in the synthesis of an aluminosilicate may lead to a metaloaluminosilicate material with similar or even greater crystallinity as its analogous aluminosilicate. Nevertheless, a decrease in aluminum quantity in the synthesis gel makes it necessary to use higher crystallization times to obtain crystalline materials [24]. This effect was also observed for [V,Al]-MCM-22 with SAR = 80 [19]. It seems that a collaborative effect between aluminum and other metal heteroatoms in the synthesis of metaloaluminosilicates exists. As far as we know, this kind of effect has not yet been studied.

[V,Al]-MCM-22 samples obtained after 192 h of hydrothermal treatment were submitted to ion-exchange procedures with Na^+ or H^+ ions, yielding the materials designated Na-[V,Al]-MCM-22 and H-[V,Al]-MCM-22. The elements concentrations in the calcined samples, determined by elemental analysis, are reported in Table 1.

Fig. 2 shows FTIR spectra of the samples obtained after different reaction times. The region of framework vibrations (1200–400 cm^{-1}) exhibited the gradual appearance of

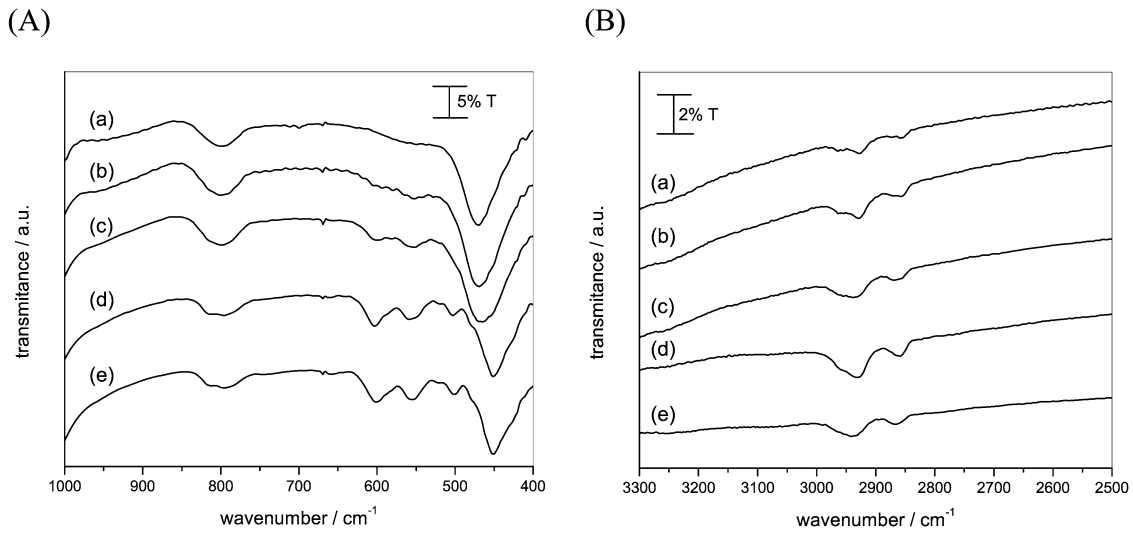

Fig. 2. FTIR spectra of as-synthesized [V,Al]-MCM-22 samples crystallized in (a) 48 h, (b) 96 h, (c) 144 h, (d) 192 h and of (e) [Al]-MCM-22 SAR = 34 at the 3300–2500 cm^{-1} region (A) and at the 1000–400 cm^{-1} region (B).

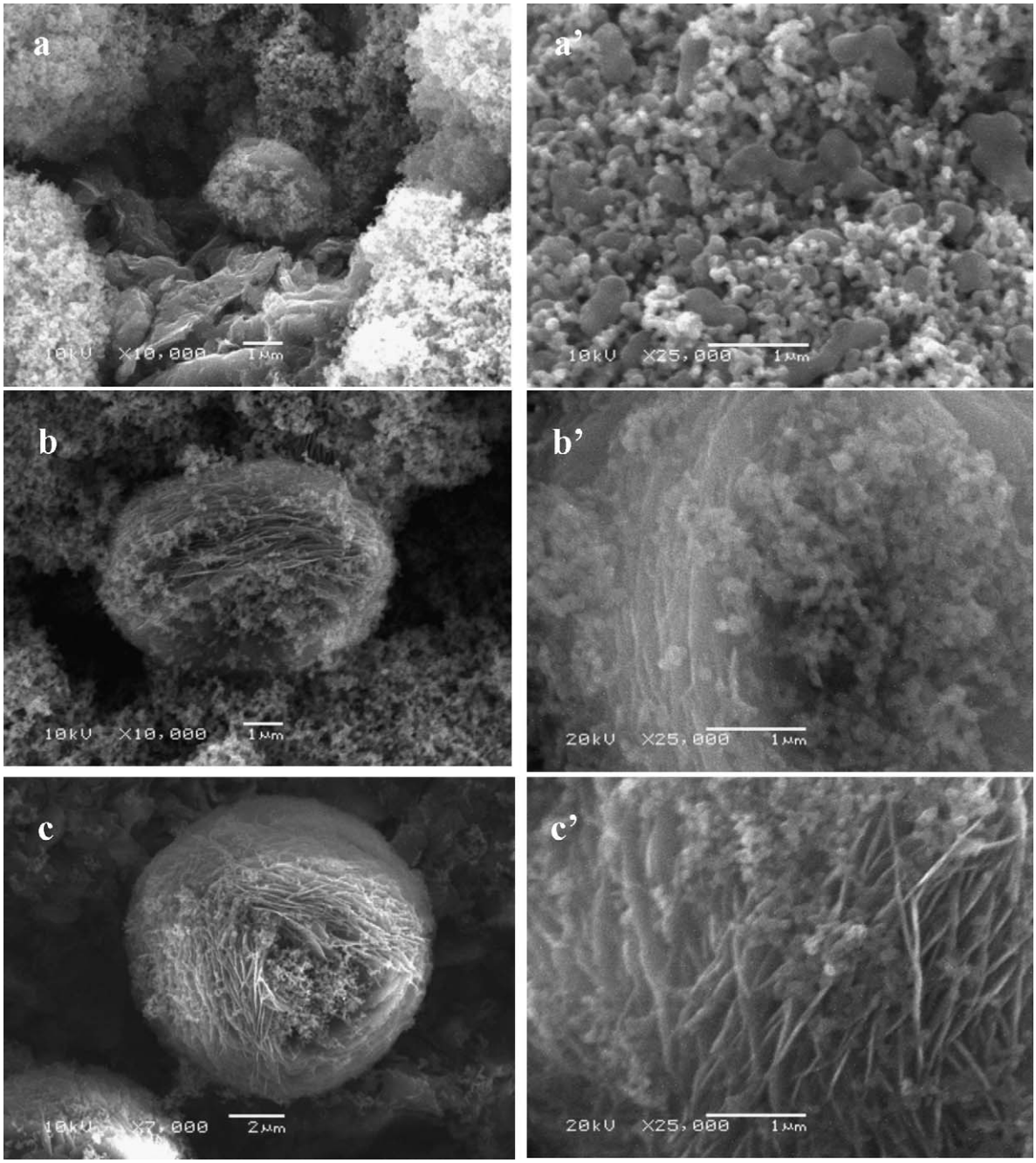

Fig. 3. SEM of as-synthesized [V,Al]-MCM-22 samples crystallized at (a) 48 h (×10,000), (a′) 48 h (×25,000), (b) 96 h (×10,000), (b′) 96 h (×25,000), (c) 144 h (×7000), (c′) 144 h (×25,000), (d) 192 h (×7000), (d′) 192 h (×25,000) and of [Al]-MCM-22 (e) ×7000 and (e′) ×25,000.

the bands due to vibration modes of the double rings (620–470 cm^{-1}) typical of the **MWW** structure (Fig. 2A). In the spectrum of the sample obtained after 48 h of synthesis (Fig. 2A, curve a), a broad weak band occurred at around 550 cm^{-1}; after 96 h, two poorly defined bands occurred at 600 and 550 cm^{-1} (Fig. 2A, curve b). Two low-intensity bands at 520 and 500 cm^{-1} appeared after 144 h, whereas the ones at 600 and 550 cm^{-1} became more resolved (Fig. 2A, curve c). Finally, after 192 h, six absorptions occurred in the IR spectrum (Fig. 2A, curve d), at 600, 560, 550, 521, 503, and 479 cm^{-1}, due to double-ring vibrations [21]. Moreover, a shift of the TO_4 tetrahedra bending mode from 470 to 450 cm^{-1}, which became more structured, between 144 h (Fig. 2A, curve c) and 192 h of synthesis time (Fig. 2A, curve d).

Fig. 2A shows the spectrum of as-synthesized [Al]-MCM-22 with SAR = 34 (curve e), which is similar to that shown found in Fig. 2A (curve d) for [V,Al]-MCM-22. However, the bands of double-ring vibrations at 620–470 cm^{-1} appear broader and less defined for [Al]-MCM-22, which is an indication of a less well-ordered system, in agreement with the XRD data (Fig. 1). Powder XRD results (Fig. 1) indicate that crystalline materials were not present until 144 h. However, the existence of organization at short distances may already be detected by FTIR at 96 h by the presence of bands corresponding to double rings.

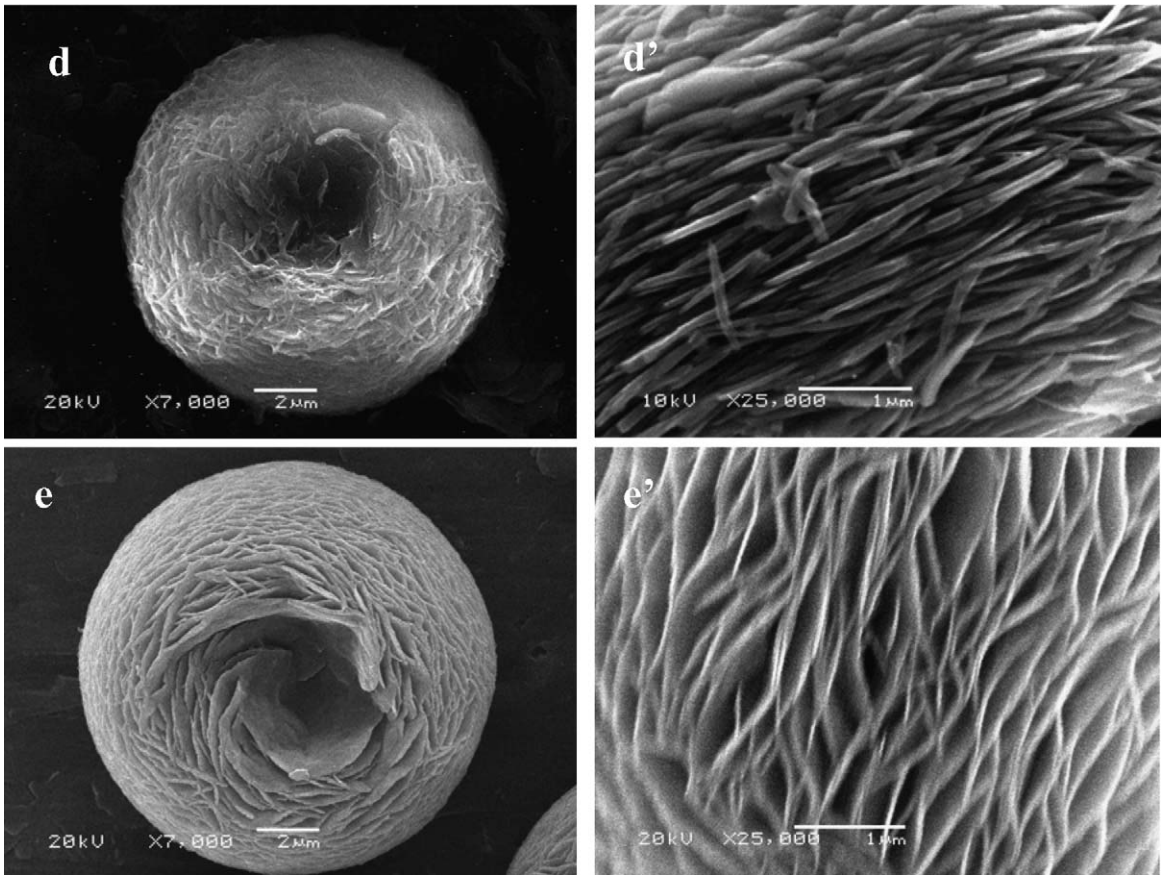

Fig. 3. (*continued*)

Nevertheless, the observation of a well-defined spectrum was possible only for the crystalline sample, obtained at 192 h.

Fig. 2B shows the CH stretching region of the organic moieties in [V,Al]-MCM-22. The general observation is that the amount of organic material retained in the solid increased as the crystallization time increased and as the product was formed. Curve a in Fig. 2B shows two pairs of bands, at 2960–2874 cm^{-1} and 2926–2858 cm^{-1}, assigned to in-phase and out-of-phase C–H vibrations of CH_2 groups of the HMI ring, with the former pair related to the two CH_2 groups closest to the NH and the latter pair related to the other four CH_2 groups. With the progress of the reaction, the bands shifted upward as a consequence of the confinement of the HMI molecules within the **MWW** framework; the more intense pair were found at 2939 and 2866 cm^{-1} in the final product, very close to those in [Al]-MCM-22 (Fig. 2B, curve e).

[V,Al]-MCM-22 crystallization was also monitored by SEM. Micrographs of samples at various crystallization times are displayed in Fig. 3. Figs. 3a and a′ show completely amorphous solids, in accordance with the results in Figs. 1a and 2A (curve a). Round particle aggregates were formed after 48 h of synthesis (Figs. 3b and c); over time, these transformed to the round, doughnut-shaped aggregates of 10–12 µm diameter (Fig. 3d). The shape and size of these aggregates are very similar to those of the [Al]-MCM-22 samples obtained by static synthesis [20]. The higher-magnification micrographs (Figs. 3a′–d′) demonstrate the gradual transformation of shapeless aggregates in the beginning of the reaction to thin homogeneous sheets after 192 h of hydrothermal treatment. Comparing the [V,Al]-MCM-22 sheets in Figs. 3d and d′ with those of [Al]-MCM-22 in Figs. 3e and e′ demonstrates that the presence of vanadium made the sheets smaller and caused tighter packing. Formation of sheet-like structures from granule-like amorphous material was already observed for [Al]-MCM-22 obtained in stirred synthesis, forming a final morphology resembling spread coins [25].

Fig. 4A displays the derivative thermogravimetric (DTG) curves of as-synthesized [V,Al]-MCM-22 samples crystallized at 48–192 h, along with a sample of as-synthesised [Al]-MCM-22 (SAR = 34) for comparison (curve e). The curves in Fig. 4A were obtained under argon; the curves in Fig. 4B, under oxygen.

Below 150 °C, the peaks refer to loss of adsorbed water. Between 150 and 370 °C, peaks are due to the decomposition of protonated HMI (H^+–HMI) and nonprotonated HMI, likely located on the 12-membered surface semicavities and in the interlamellar region and between 370 and 520 °C HMI and H^+–HMI in the sinusoidal bidimensional 10-membered channels. Finally, above 520 °C, dehydroxylation and/or desorption of residues produced by HMI fragmentation at high temperatures occurred [20]. Table 2 lists the percentages of mass losses determined by TGA at the different temperature ranges, under argon and under oxygen.

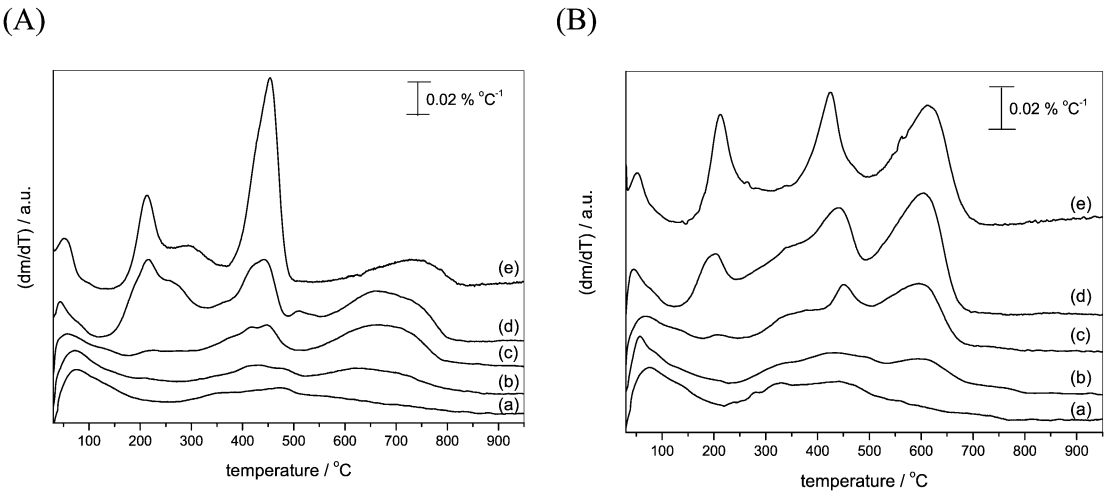

Fig. 4. DTG curves of as-synthesized [V,Al]-MCM-22 samples crystallized in (a) 48 h, (b) 96 h, (c) 144 h, (d) 192 h and [Al]-MCM-22 (e) under argon (A) and (B) under oxygen.

Table 2
Percentage of mass losses, determined by TGA

	30–150 °C (%)		150–370 °C (%)		370–520 °C (%)		520–1000 °C (%)		Total (%)	
	Ar	O_2	Ar	O_2	Ar	O_2	Ar	O_2	Ar	O_2
[V,Al]-MCM-22 48 h	2.3	2.3	2.3	2.9	2.2	2.6	2.3	1.7	9.0	9.6
[V,Al]-MCM-22 96 h	2.2	2.1	2.2	2.2	2.4	2.8	3.7	2.8	10.5	9.8
[V,Al]-MCM-22 144 h	1.7	1.6	2.4	2.5	2.9	3.8	5.5	4.7	12.5	12.6
[V,Al]-MCM-22 192 h	1.5	1.4	7.0	5.7	5.1	6.1	6.9	7.4	20.5	20.7
[Al]-MCM-22	1.9	1.4	5.7	5.0	8.1	5.6	4.3	7.3	20.0	19.4

The results in Fig. 4 and Table 2 indicate that as [V,Al]-MCM-22 crystallized, the amount of water and organic material retained in the solid increased. Simultaneously, the amount of water released from the solids with temperature decreased as the structure was formed under either argon or air. This indicates that the gel was more hydrophilic than the [V,Al]-MCM-22 and/or the number of water adsorption sites diminished on crystallization as Si–OH groups were transformed to siloxane bridges (Si–O–Si groups). The increasing smaller amount of adsorbed water was paralleled by an increase in the retained organic material as specific zeolitic sites were being formed, as already noted for XRD and IR results.

Another point to note is that the amount of mass loss in the 150–370 °C region was approximately constant for materials crystallized at 48–144 h; after 192 h, however, the mass lost in this temperature range increased significantly. This effect is related to the decomposition of HMI in the semicavities and the interlamellar region. The loss occurring at 370–520 °C, on the other hand, increased with increasing reaction time in a smoother fashion. This finding demonstrates that the formation of the sinusoidal bidimensional channels, and the incorporation of HMI inside them, occurred before the organization into a lamellar material. This finding is in line with the formation of MCM-56, a material obtained from the same synthesis mixtures as MCM-22 but collected at shorter reaction times [26]. MCM-56 corresponds to an MCM-22 in which the layers are randomly distributed. Organization of layers must be the predominant phenomenon in the last 48 h of reaction. This result is in accordance with FTIR results, which show major incorporation of HMI occurring in the last 48 h of reaction (Fig. 2A), even when organization at short distances in the materials crystallized in shorter time periods was already observed (Fig. 2B).

Under argon, [V,Al]-MCM-22 (192 h) had a slightly higher total mass loss in comparison to [Al]-MCM-22 (Table 2), and both samples had DTG peaks at about the same temperatures (Fig. 4A). In the case of [V,Al]-MCM-22, the band at ∼450 °C was split into two bands, with a component at 510 °C. [V,Al]-MCM-22 also had a higher percentage of mass loss above 520 °C (Table 2). For [V,Al]-MCM-22, a component of the band in the 520–1000 °C region was centered at 650 °C, which is almost absent for [Al]-MCM-22 (compare curves d and e in Fig. 4A), meaning that desorption found in this region for [V,Al]-MCM-22 should have remained relative to the decomposition of HMI in the sinusoidal channels, a part of which desorbed/decomposed in the 370–520 °C region. In fact, a much greater fraction of organic material decomposed at higher temperature in the [V,Al]-MCM-22 192-h sample than in the [Al]-MCM-22 192-h sample (36.3% vs. 23.7%). Therefore, the presence of vanadium ions seems to produce different fragmentation patterns or different products that desorb/decompose at higher temperatures compared with the material that does not contain vanadium.

The presence of structural vanadium in molecular sieves led to changes in template-framework interaction. This effect was already observed for vanadoaluminophosphates (VAPOs) in comparison to their analogous aluminophosphates (ALPOs).

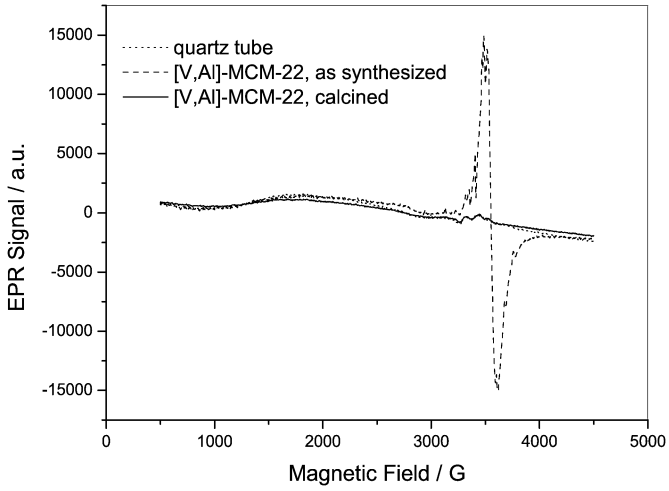

Fig. 5. EPR spectra of as-synthesized (a) and calcined (b) [V,Al]-MCM-22 (192 h) samples and of the empty quartz tube (c).

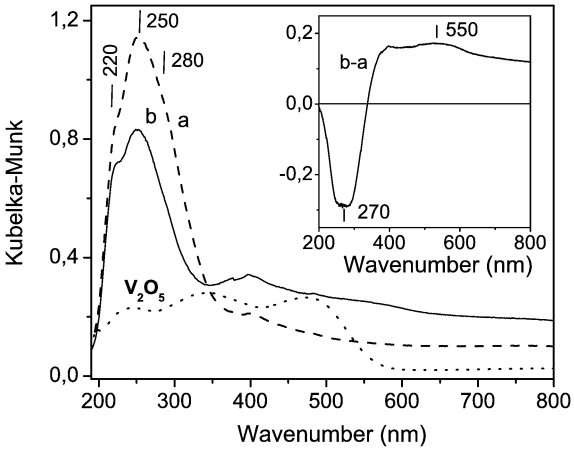

Fig. 6. DR–UV–vis spectra of [V,Al]-MCM-22 oxidized at 580 °C (curve a, dashed line) and reduced at 500 °C (curve b, solid line); after the treatments the samples were evacuated at 250 and 500 °C, respectively. The spectrum of pure V_2O_5 (conveniently divided for a factor of ten) has been added for comparison (dotted line). The inset shows the result of the subtraction of the spectra (b-a).

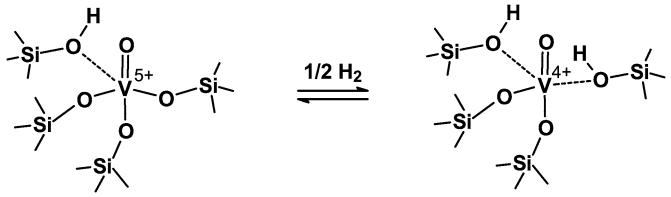

Scheme 1

In VAPOs, the presence of small quantities of vanadium in the framework caused the materials to present four mass losses instead of three, as was observed for ALPOs [27]. For VAPOs, part of the decomposition of the template occurred at higher temperatures, as for [V,Al]-MCM-22 in comparison to [Al]-MCM-22. Moreover, [V,Al]-MCM-22 had a higher total mass loss than [Al]-MCM-22 with similar SAR (20.7% vs. 19.4%). Thus, both the stronger template-framework interaction and the greater quantity of template molecules inserted in the material may be responsible for the higher crystallinity of the vanadoaluminosilicate, as determined by XRD (Fig. 1).

Under oxygen (Fig. 4B), the differences between [V,Al]-MCM-22 and [Al]-MCM-22 are less pronounced than those in argon; in fact, in all temperature ranges, both samples had similar mass losses. The major differences, in terms both of mass losses and maximum rate of mass losses, occurred in the 150–370 and 370–520 °C ranges. It is, however, difficult to determine whether these differences were due to the presence of vanadium or to the slightly different crystallinity of the two samples. This means that the HMI molecules should monitor different degrees of constraint in the [V,Al]-MCM-22 and [Al]-MCM-22 samples. We mentioned for completeness that the different behaviors at higher temperatures observed under argon also could possibly be assigned to the different crystallinity of the two samples.

EPR spectra of [V,Al]-MCM-22 synthesized in 192 h show that the as-synthesized material (Fig. 5, curve a) contained paramagnetic V^{4+} ions, which, after calcination, were completely oxidized to EPR-silent V^{5+}. The EPR signal was in fact absent after calcination. Although V^{4+} ions in the as-synthesized material were not quantified, they seemed to exist in a greater extent in comparison with other V-containing zeolites studied earlier [12]. This observation supports our previous findings by DR–UV–vis spectroscopy [18].

Fig. 6 shows the DR–UV–vis spectra of [V,Al]-MCM-22 submitted to oxidation at 580 °C under O_2 (curve a) and subsequently to reduction at 500 °C under H_2 (curve b). Broad absorption was present in the spectrum of the oxidized [V,Al]-MCM-22 (Fig. 6, dashed line) with a maximum at 250 nm and shoulders at 220 and 270–300 nm. These absorptions were assigned to the oxygen to V^{5+} charge transfer (CT) transition in distorted (pseudo)tetrahedral oxovanadium $(SiO)_3V{=}O$ species [11,12,28,29].

On reduction, the spectrum of [V,Al]-MCM-22 decreased in intensity (20–30%), especially at higher wavelengths, and a very broad absorption of V^{4+} d–d transition was formed at wavelengths above 350 nm (Fig. 6, solid line). A subtraction between the two DR–UV–vis spectra obtained after reduction and oxidation (Fig. 6, inset) showed a weak, broad band at around 550 nm formed in parallel to the decreased signal at 270 nm. This effect is almost completely reversible, and several cycles were made to ensure that this phenomenon is reliable and reproducible. This behavior was described in previous contributions [18,19] in terms of transformation (Scheme 1) of distorted tetrahedral V^{5+} ions (band at 270 nm) into V^{4+} species (band at 550 nm). This transformation is reversible, with the intensity of the V^{5+} charge transfer being almost completely restored on reoxidation. The redox behavior of [V,Al]-MCM-22 has been fully confirmed with the aid of FTIR of CO adsorbed at 100 K (vide infra).

Finally, we mention that the DR–UV–vis spectra of both reduced and oxidized samples showed very weak and broad absorptions at around 400 and 480 nm. These absorptions, which are not always found in [V,Al]-MCM-22 samples, have been assigned to extra-framework VO_x oligomeric species [18]. The presence of purely stoichiometric V_2O_5 extraphase is not fully

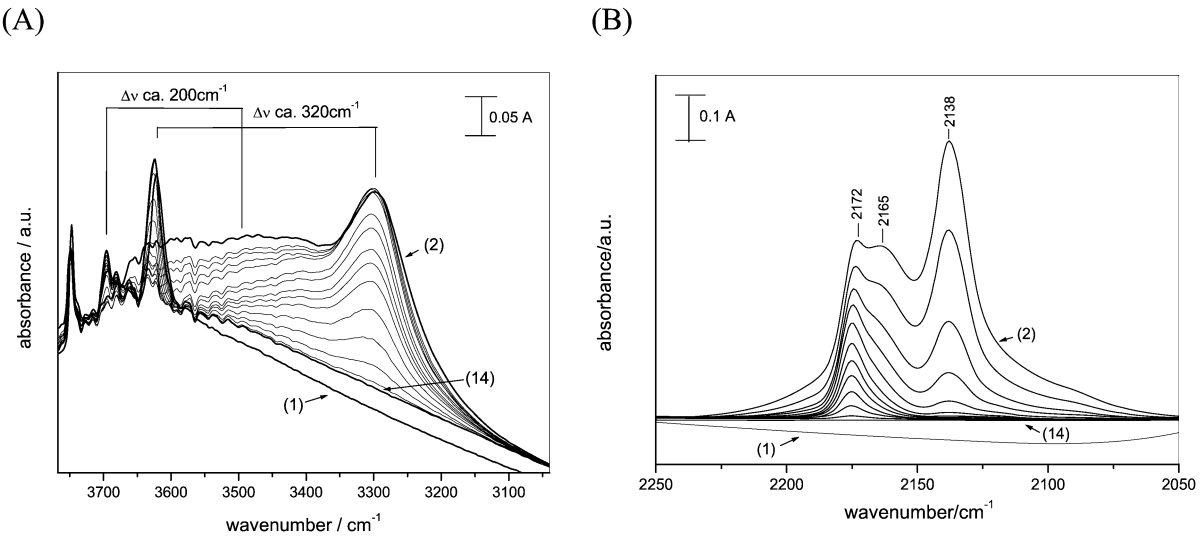

Fig. 7. FTIR spectra in the hydroxyl stretching region (A) and in the CO stretching region (B) before (curve 1) and after (curve 2) CO adsorption at 100 K on oxidized [V,Al]-MCM-22. The curves correspond to decreasing CO doses from 40 Torr (curve 2) to 1×10^{-2} Torr (curve 14). Difference spectra of adsorbed CO are presented after subtraction of the spectrum of the bare sample (curve 1).

convincing in that its spectrum (Fig. 6) shows maxima at different positions [11]. However, the band edge energy of V(V) oxides depends on, among other factors, the number of V–O–V bonds in the coordination sphere of the central V(V) cation (i.e., the degree of aggregation/polimerization of the absorbing species).

This effect was carefully studied by Gao and Wachs, who reported a DR UV–vis–NIR study of several V_2O_5 supported oxides and reference V(V) compounds [30]. Based on their findings, which demonstrated that the molecular structures of the surface vanadium oxide species strongly depended on the support and vanadia loading (e.g., the surface density), defining the precise molecular nature/structure of the aggregates absorbing at around 400 nm in [V,Al]-MCM-22 is rather difficult. These species, which are probably small clusters of vanadium oxides either inside the **MWW** cages or outside the zeolite particles aggregates, represent only a minor fraction of the overall vanadium ions or, more importantly, do not affect the redox behavior of the catalyst. It is in fact evident (Fig. 6, inset) that the absorption at 400 nm did not change significantly after the oxidation/reduction cycle.

Fig. 7A shows the spectra in the stretching hydroxyl region of the calcined sample obtained before and after CO adsorption at 100 K. This experiment was used to monitor both the acidity of the hydroxyls and the Lewis acidity of the [V,Al]-MCM-22 199-h sample. Silanols, hydroxyls of partially-extra-framework aluminum ions, and bridged hydroxyls were found in the spectrum of the bare calcined sample at 3749, 3700–3650, and 3624 cm^{-1}, respectively [19,31]. Hydroxyls surrounding the vanadium centers of [V,Al]-MCM-22, as proposed in Scheme 1, were also found to absorb at around 3695 cm^{-1} [19].

On CO adsorption, a downward shift of the bridged hydroxyls at around 320 cm^{-1} was observed on both the oxidized and reduced sample, demonstrating a strong, broad band at around 3300 cm^{-1}. A shift of 320 cm^{-1} on pure [Al]-MCM-22 was also found in previous studies [31], suggesting that the vanadium sites have no significant effects on the bridged Si(OH)Al groups, which are the strongest Brønsted acid sites in the [Al]-MCM-22 zeolite.

Besides the strong band at around 3300 cm^{-1} due to CO H-bonded to bridged hydroxyls, a very broad and composite absorption at 3600–3350 cm^{-1} was formed on CO adsorption at 100 K. In the oxidized sample, the formation of this broad absorption centered at around 3500 cm^{-1} was assigned to CO bonded to silanols interacting with V^{5+} centers (Schemes 1 and 2). The presence of this band, as well as the comparison with the spectra of the reduced sample, was well described previously [19]. On CO adsorption, hydroxyls of partially extra-framework aluminum absorbed at 3600–3400 cm^{-1}, similar to silanols interacting with V^{5+}. This makes the assignment of the two different hydroxyls rather uncertain. Scheme 2 shows the possible acidic sites in [V,Al]-MCM-22, the ν_{OH} after CO adsorption and the shift $\Delta\nu_{OH\cdots CO}$ for each site.

In the CO stretching frequency region (Fig. 7B), along with the CO bound to bridged hydroxyls (band at 2172 cm^{-1}) and the absorption of physisorbed, liquid-like CO (band at 2138 cm^{-1}) [32,33], a broad band at 2165 cm^{-1} was also found at high CO doses on the oxidized sample. Absorptions in this position were assigned to CO bound to Al–OH in partially dealuminated MCM-22 [31]. Both the intensity and width of the bands at 2175–2150 cm^{-1} suggest that these absorptions have a composite nature. It has been proposed that the stretching of CO adsorbed on the silanols bonded to the oxovanadium species also falls in this region [19].

A very interesting result was found by comparing the spectra of the oxidized and reduced [V,Al]-MCM-22 sample taken on very low CO dosages. A band at 2190 cm^{-1} was observed for the reduced [V,Al]-MCM-22 sample, which was not present in the oxidized sample (Fig. 8). The presence of this band is probably due to the coordination of CO with V^{4+} Lewis sites. These results are in agreement with literature data showing that V^{5+} species do not adsorb CO even at low temperatures, and

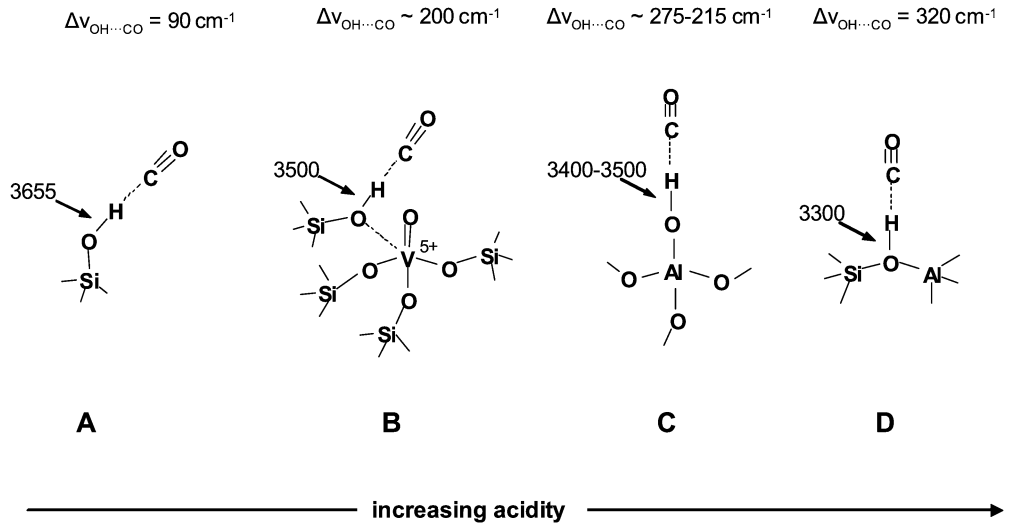

Scheme 2

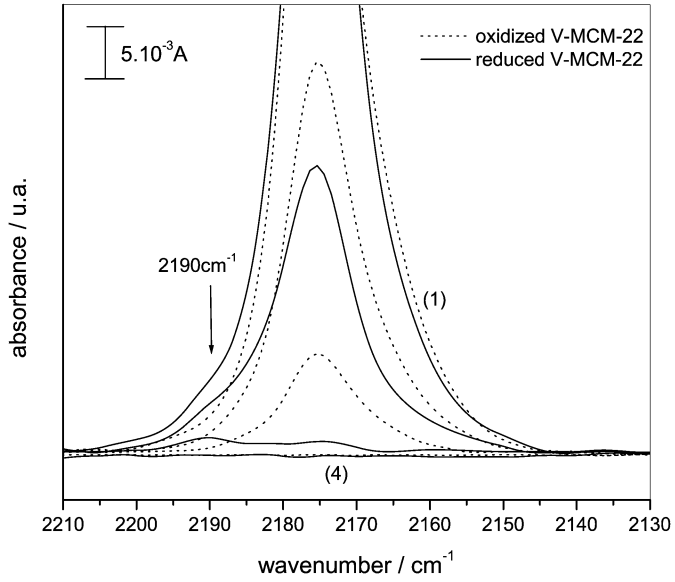

Fig. 8. FTIR spectra of [V,Al]-MCM-22 in the hydroxyl stretching region after CO adsorption at 100 K at low coverages on oxidized (dashed line) and reduced (solid line) [V,Al]-MCM-22. The curves correspond to decreasing CO doses from 4×10^{-2} Torr (curves 1) to 1×10^{-2} Torr (curves 4).

that V^{4+} form carbonyl complexes in the 2212–2180 cm^{-1} region that are not stable to evacuation of the samples [34,35]. These results are also in accordance with our DR–UV–vis results demonstrating that V^{4+} centers are present only in the reduced samples.

Preliminary catalytic tests of oxidative dehydrogenation (ODH) of propane were performed for H-[V,Al]-MCM-22 and Na-[V,Al]-MCM-22. The catalysts H-[Al]-MCM-22 (SAR = 60) and Na-[Al]-MCM-22 (SAR = 62, Na/Al = 0.28) were used for comparison with the samples not containing vanadium (Figs. 9A and B). For all of the catalysts, the main products were propene, CO, and CO_2, along with a nonnegligible amount of methane related to the cracking activity of zeolites. Performance was comparable to that reported in the literature for zeolites containing higher concentrations of vanadium [36]. Furthermore, it also should be emphasized that catalysts not containing vanadium were active for the reaction, demonstrating that the zeolite had its own intrinsic activity that was very similar for H-[Al]-MCM-22 and the Na-exchanged sample (4.54×10^{-7} mol C_3H_8 reacted $g^{-1}\,s^{-1}$ and 4.22×10^{-7} mol C_3H_8 reacted $g^{-1}\,s^{-1}$, respectively, at 500 °C). For both samples, the incorporation of vanadium in the structure resulted in enhanced catalytic activity (6.32×10^{-7} mol C_3H_8 reacted $g^{-1}\,s^{-1}$ and 8.38×10^{-7} mol C_3H_8 reacted $g^{-1}\,s^{-1}$, respectively, at 500 °C). Nevertheless, because of negative effect on propene selectivity, vanadium insertion increased propene productivity only for the Na-substituted catalyst (1.68×10^{-7} mol C_3H_6 produced $g^{-1}\,s^{-1}$ for Na-[Al]-MCM-22 vs. 2.77×10^{-7} mol C_3H_6 produced $g^{-1}\,s^{-1}$ for Na-[V,Al]-MCM-22 evaluated at 500 °C). This likely can be attributed to the reduction of very strong Brønsted acid sites by alkaline ion exchange inhibiting cracking reactions, as suggested by the lower methane formation observed for the Na-exchanged samples.

In conclusion, MCM-22 is active in the ODH of propane, with improved catalytic performance due to the simultaneous presence of vanadium and an alkaline metal neutralizing a fraction of the zeolite acid sites. Because of the synergic effect of vanadium and sodium, a quantitative attribution of a fraction of catalytic activity to the incorporated vanadium cannot be made; however, the results presented in this paper indicate that structural V atoms change the catalytic characteristics of [Al]-MCM-22 and may provide interesting catalysts for oxidation reactions.

4. Conclusion

The insertion of vanadium ions into **MWW** framework was successfully conducted. As-synthesized [V,Al]-MCM-22 crystallized in 192 h under static conditions had similar morphology to [Al]-MCM-22 and contained V^{4+} species that were oxidized to V^{5+} ions when calcined under oxygen at 580 °C. Monitoring of crystallization led to the proposition that the **MWW** layers

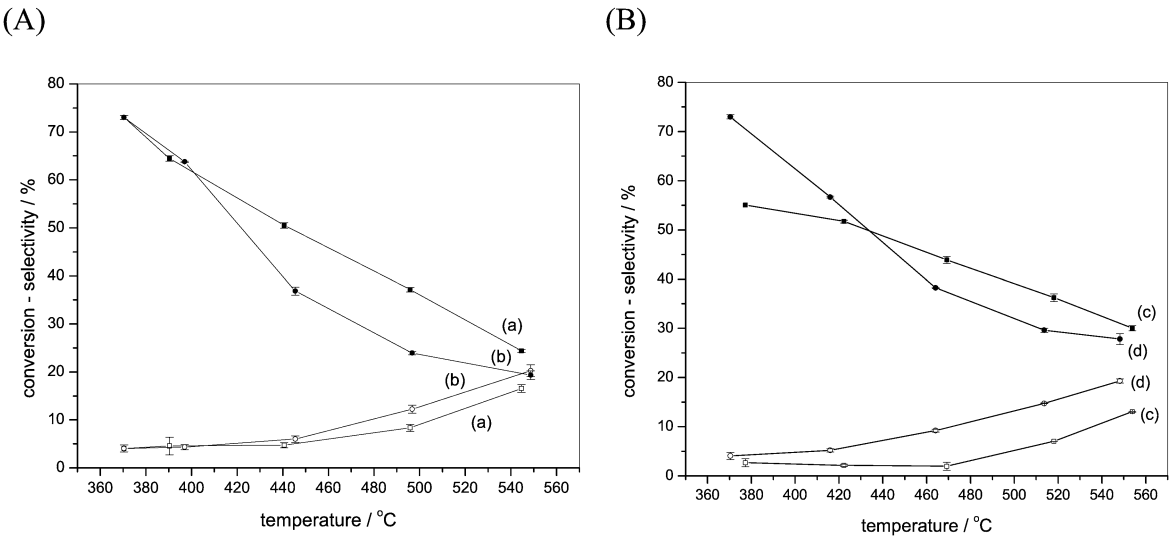

Fig. 9. Conversion of propane (open symbols) and selectivity to propene (full symbols) for (a) H-[Al]-MCM-22, (b) H-[V,Al]-MCM-22 (panel A), (c) Na-[Al]-MCM-22, and (d) Na-[V,Al]-MCM-22 (panel B), catalysts on propane ODH reaction.

are formed in the first hours of reaction with their organization occurring at the end of the reaction.

The V^{5+} species present in both calcined and Na^{+}-exchanged samples may be reduced under hydrogen at 500 °C, and the reduced species can be detected by DR–UV–vis spectroscopy and FTIR with adsorption of CO. This redox behavior is reversible, with the V^{4+} ions being reoxidized to V^{5+} under oxygen at 580 °C.

Both reduced and oxidized samples showed Brønsted acidity due to protons located at the OH bridged to silicon and aluminum and to partial extra-framework Al ions. V^{4+} Lewis acid sites were found on reduced samples that very weakly bound CO adsorbed at 100 K. Na^{+}-exchanged [V,Al]-MCM-22 and [Al]-MCM-22 tested in the ODH of propane and demonstrated similar performance to other zeolites containing higher concentrations of vanadium. Na-[V,Al]-MCM-22 was twice as active in propane conversion than Na-[Al]-MCM-22.

Acknowledgments

The authors acknowledge support from the Brazilian Fundação de Amparo à Pesquisa no Estado de São Paulo (FAPESP) and the Italian Ministero dell'Istruzione, dell'Università e della Ricerca (project FIRB2001). A.A. also acknowledges FAPESP and the Coordenação de Aperfeiçoamento de Pessoal de Nivel Superior for fellowships. The authors thank Prof. Ana Maria Ferreira (IQ-USP, Brazil), Prof. José Salvador Barone (IQ-Unicamp, Brazil), Dr. Érico Teixeira Neto (Oxiteno, Brazil), and Dr. Chiara Bisio for help with EPR, elemental analysis, SEM, and DR–UV–vis, respectively.

References

[1] M.K. Rubin, P. Chu, US Patent 4,959,325 (1990).
[2] A. Corma, V. Fornés, J.M. Guil, S. Pergher, T.L.M. Maesen, J.G. Buglass, Microporous Mesoporous Mater. 38 (2000) 301.
[3] C.T. Kresge, W.J. Roth, US Patent 5,310,715 (1994).
[4] S.J. Kim, K. Jung, O. Joo, J. Porous Mater. 11 (2004) 211.
[5] P. Wu, T. Tatsumi, T. Komatsu, T. Yashima, J. Phys. Chem. B 105 (2001) 2897.
[6] F. Testa, F. Crea, G.D. Diodati, L. Pasqua, R. Aiello, P. Lentz, J.B. Nagy, Microporous Mesoporous Mater. 30 (1999) 187.
[7] G. Berlier, M. Pourny, S. Bordiga, G. Spoto, A. Zecchina, C. Lamberti, J. Catal. 229 (2005) 45.
[8] P. Wu, T. Tatsumi, T. Komatsu, T. Yashima, J. Catal. 202 (2001) 245.
[9] P. Wu, Y. Liu, M. He, T. Komatsu, T. Tatsumi, J. Catal. 228 (2004) 183.
[10] R.A. Morrisson, M.K. Rubin, US Patent 5,284,643 (1994).
[11] G. Centi, S. Perathoner, F. Trifirò, A. Abukais, C.F. Aissi, M. Guelton, J. Phys. Chem. 96 (1992) 2617.
[12] M. Wark, M. Koch, A. Brückner, Grünert, J. Chem. Soc., Faraday Trans. 94 (1998) 2033.
[13] S. Dzwigaj, M. Matsuoka, M. Anpo, M. Che, J. Phys. Chem. B 104 (2000) 6012.
[14] A.M. Prakash, L. Kevan, J. Phys. Chem. B 104 (2000) 6860.
[15] P.R. Hari Prasad Rao, A.V. Ramaswamy, P. Ratnasamy, J. Catal. 137 (1992) 225.
[16] M.S. Rigutto, H. van Bekkum, Appl. Catal. 68 (1991) L1.
[17] P.J. Carl, S.L. Isley, S.C. Larsen, J. Phys. Chem. A 105 (2001) 4563.
[18] A. Albuquerque, H.O. Pastore, L. Marchese, Stud. Surf. Sci. Catal. 158 (2005) 901.
[19] A. Albuquerque, H.O. Pastore, L. Marchese, Stud. Surf. Sci. Catal. 155 (2005) 45.
[20] A.L.S. Marques, J.L.F. Monteiro, H.O. Pastore, Microporous Mesoporous Mater. 32 (1999) 131.
[21] A. Corma, C. Corell, J. Pérez-Pariente, J.M. Guil, R. Guil-López, S. Nicolopoulos, J. Gonzalez-Calbet, M. Vallet-Regi, Zeolites 16 (1996) 7.
[22] S.S. Shevade, B.S. Rao, J. Mater. Chem. 9 (1999) 2459.
[23] A. Tavolaro, P. Tavolaro, E. Drioli, J. Cryst. Growth 289 (2006) 609.
[24] F. Testa, F. Crea, G.D. Diodati, L. Pasqua, R. Aiello, G. Terwagne, P. Lentz, J.B. Nagy, Microporous Mesoporous Mater. 30 (1999) 187.
[25] I. Mochida, S. Eguchi, M. Hironaka, S. Nagao, K. Sakanishi, D.D. Whitehurst, Zeolites 18 (1997) 142.
[26] A.S. Fung, S.L. Lawton, W.J. Roth, US Patent 5,362,697 (1994).
[27] N. Venkatathri, Appl. Catal. A 242 (2003) 393.
[28] T. Sen, P.R. Rajamohanan, S. Ganapathy, S. Sivasanker, J. Catal. 163 (1996) 354.
[29] C.A. Trujillo, U.N. Uribe, P. Knops-Gerrits, L.A. Oviedo, P.A. Jacobs, J. Catal. 168 (1997) 1.
[30] X. Gao, I.E. Wachs, J. Phys. Chem. B 104 (2000) 1261.
[31] B. Onida, F. Geobaldo, F. Testa, F. Crea, E. Garrone, Microporous Mesoporous Mater. 30 (1999) 119.

[32] S. Bordiga, E.E. Platero, C.O. Areán, C. Lamberti, A. Zecchina, J. Catal. 137 (1992) 179.
[33] J. Kristóf, J. Mink, E. Horváth, M. Gábor, Vib. Spectrosc. 5 (1993) 69.
[34] P. Concepción, K. Hadjiivanov, H. Knözinger, J. Catal. 184 (1999) 172.
[35] P. Concepción, H. Knözinger, J.M. López Nieto, A. Martínez-Arias, J. Phys. Chem. B 106 (2002) 2574.
[36] G. Centi, F. Trifirò, Appl. Catal. 143 (1996) 3.